David Zimmerman

Prof. Ron Dror

BIOPHYS 279

4 December 2015

Image Analysis of Radiation-Induced DNA Damage in Adult *Drosophila* Brain Tissue

1. Introduction

Genomic DNA is under constant assault from a wide variety of processes, both endogenous and environmental.[1,2] DNA double-strand breaks (DSBs) are an especial threat to genomic integrity because of their propensity to cause chromosomal rearrangements and other similarly deleterious mutations.[3–5] As such, defects in the DSB-repair machinery are associated with many pathologies ranging from cancer to neurodegeneration.[5–10] DSBs have also been implicated in physiologic processes like V(D)J recombination, meiotic crossover, and transcriptional regulation through chromatin remodeling.[4,11,12]

In mammals, an early stage of the signaling and repair response to DSBs involves phosphorylation of histone variant H2A.X at serine 139 to yield γ-H2A.X.[13,14] This modified histone is then recruited to the site of the lesion, which stimulates the modification and recruitment of additional histones in a positive feedback loop that leads to accumulation of γ-H2A.X in foci extending many megabases from the DSB.[15,16] Furthermore, these puncta, which have been shown to correspond one-to-one with individual DSBs, can be detected by immunostaining and resolved/enumerated microscopically.[13–16]

In what follows, I will present an analysis of γ-H2A.V (the invertebrate homolog of γ-H2A.X) immunofluorescence in images obtained by confocal microscopy of fixed brain tissue from the adult fruit fly *Drosophila melanogaster*. In particular, I will characterize the

physiologic response to DSBs caused by varying doses of ionizing radiation (IR) by examining the size, intensity, and distribution of γ-H2A.V foci within cell nuclei.[5] In this, flies are a useful model system, because of the relative simplicity of their invertebrate physiology. Their small size is also advantageous in a particular experimental way: approximating tissue as water—with density $\rho = 1\ \mathrm{g/cm^3}$ and mass attenuation coefficient $\mu/\rho = 0.17\ \mathrm{cm^2/g}$ for light of energy $h\nu = 100$ keV—we estimate an attenuation length of

$$\mu^{-1} = \frac{1}{(0.17\ \mathrm{cm^2/g})(1\ \mathrm{g/cm^3})} = 5.9\ \mathrm{cm}.$$

If we suppose the radius of a fruit fly (assuming a spherical fruit fly!) to be roughly 1 mm, we see that the length scale for attenuation of incident x-rays is almost two orders of magnitude larger.[17] Therefore, if one were to aim a beam of x-rays at a fruit fly, one would expect the intensity of the beam (and the flux of photons) to be roughly uniform throughout the fly; that is, it is justifiable to treat the fly as a point for the purpose of analyzing IR dose responses.

2. Materials and Methods

Wild-type (isogenic) female flies were collected five days after eclosion, immobilized, and irradiated on ice with a Torrex 120D x-ray source (100 kV, 4 mA). Dosage was modulated by varying the time of exposure between 16 s (2 Gy) and 160 s (20 Gy). Afterward, the flies were allowed to recover at 25 °C for 20 min, after which their brains were immediately dissected, fixed, and stained with a rabbit anti-γ-H2A.V polyclonal antibody (1:500) using a standard protocol.[5] After incubation in secondary antibody solution, brains were counterstained with DAPI (0.5 μg/mL) to label nuclei and transferred to 70% glycerol overnight. The next day, brains were mounted in Vectashield using coverslip spacers and imaged on an upright confocal laser scanning microscope (Leica TCS SP8). Optical sections of 1 μm in thickness were taken through the anterior medulla cortex.

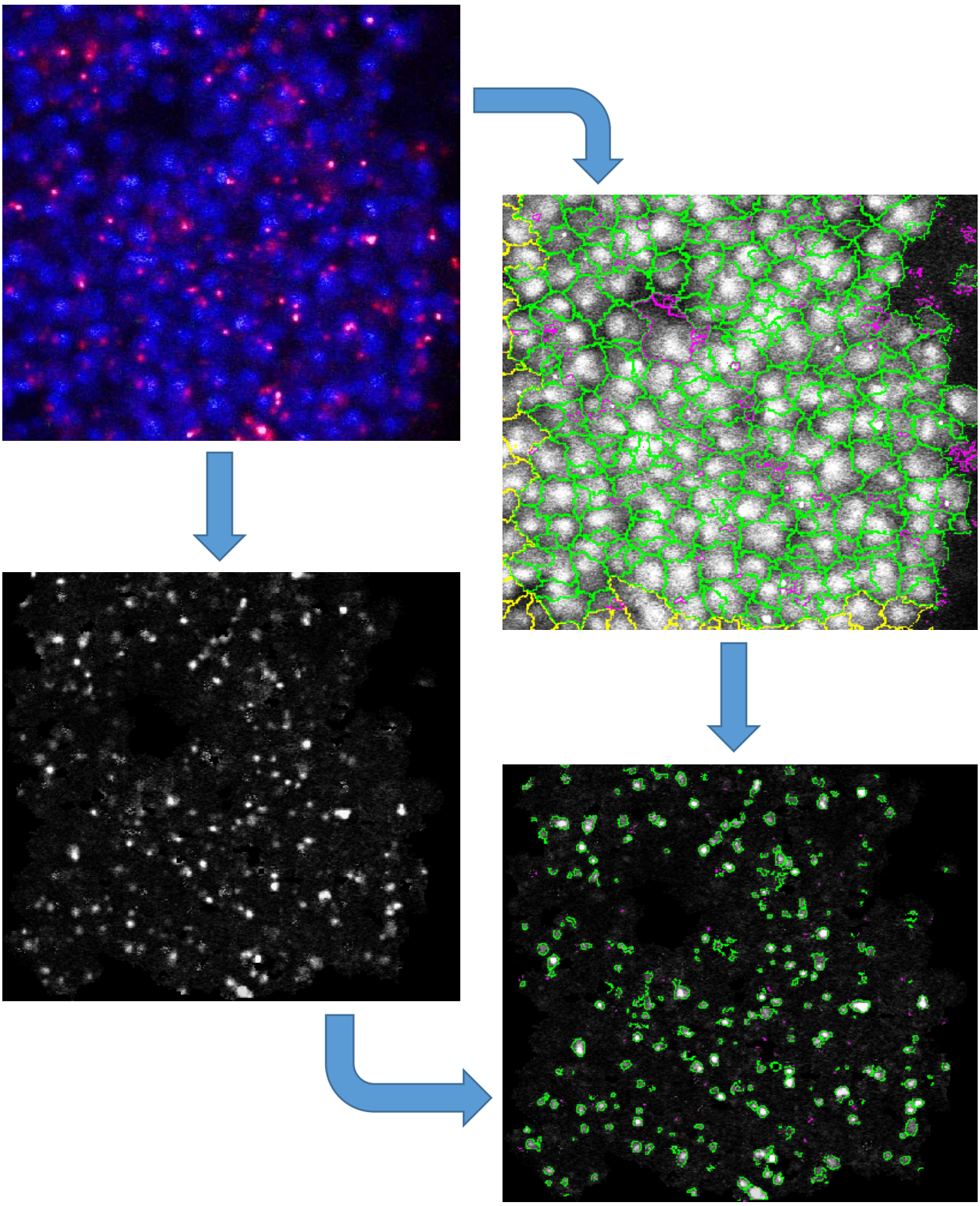

Figure 0. Representative workflow of automated image processing and analysis in CellTool. Top left: original image (channels superimposed). Top right: segmentation analysis of DAPI (blue) channel to create nuclear mask. Bottom left: conversion of γ-H2A.V (red) channel to grayscale for enhancement of punctate features. Bottom right: identification and measurement of individual γ-H2A.V foci.

After image acquisition, CellProfiler 2.1.1 was used to create an analysis pipeline for the purpose of extracting salient features of γ-H2A.V structure and distribution from the optical sections.[18] First, the multichannel RGB images generated by the microscope were split into separate gray channels. Cell nuclei were then identified and enumerated in the DAPI channel by global thresholding using Otsu's method, followed by application of a smoothing filter for declumping. Then, the nuclei were subjected to segmentation analysis by a strategy consisting of three steps: 1) determine if a (threshold-defined) foreground region comprises a single nucleus or multiple nuclei; 2) identify edges of nuclei; 3) reject nuclei that fall outside of size range, touch the image borders, or contain a local maximum less than 9 pixels from that of another nucleus.

Subsequent image processing steps included enhancement and identification of punctate features in the γ-H2A.V channel (after convolution with the nuclear mask), measurement of object sizes and intensities, and association of individual foci to parent nuclei. Using a MATLAB script, the output files generated by CellProfiler were parsed and the data extracted. Data from multiple optical sections of the same brain were pooled (on the assumption of homoscedasticity) and subjected to correlation analysis and linear regression, as described in greater detail below.

3. Results and Discussion

For a given dose of radiation, we may suppose that every internucleotide phosphodiester bond has the same very small probability of developing a DSB. However, there is obviously a very large amount of DNA in a fly brain. Thus, the number of γ-H2A.V foci per nucleus should be described by a Poisson distribution.[19] To test this hypothesis, histograms were generated from the foci counts obtained after irradiating flies with 0, 2, 10, and 20 Gy of x-rays. Each empirical frequency distribution was then fit to a Poisson probability mass function of parameter λ corresponding to the sample mean.

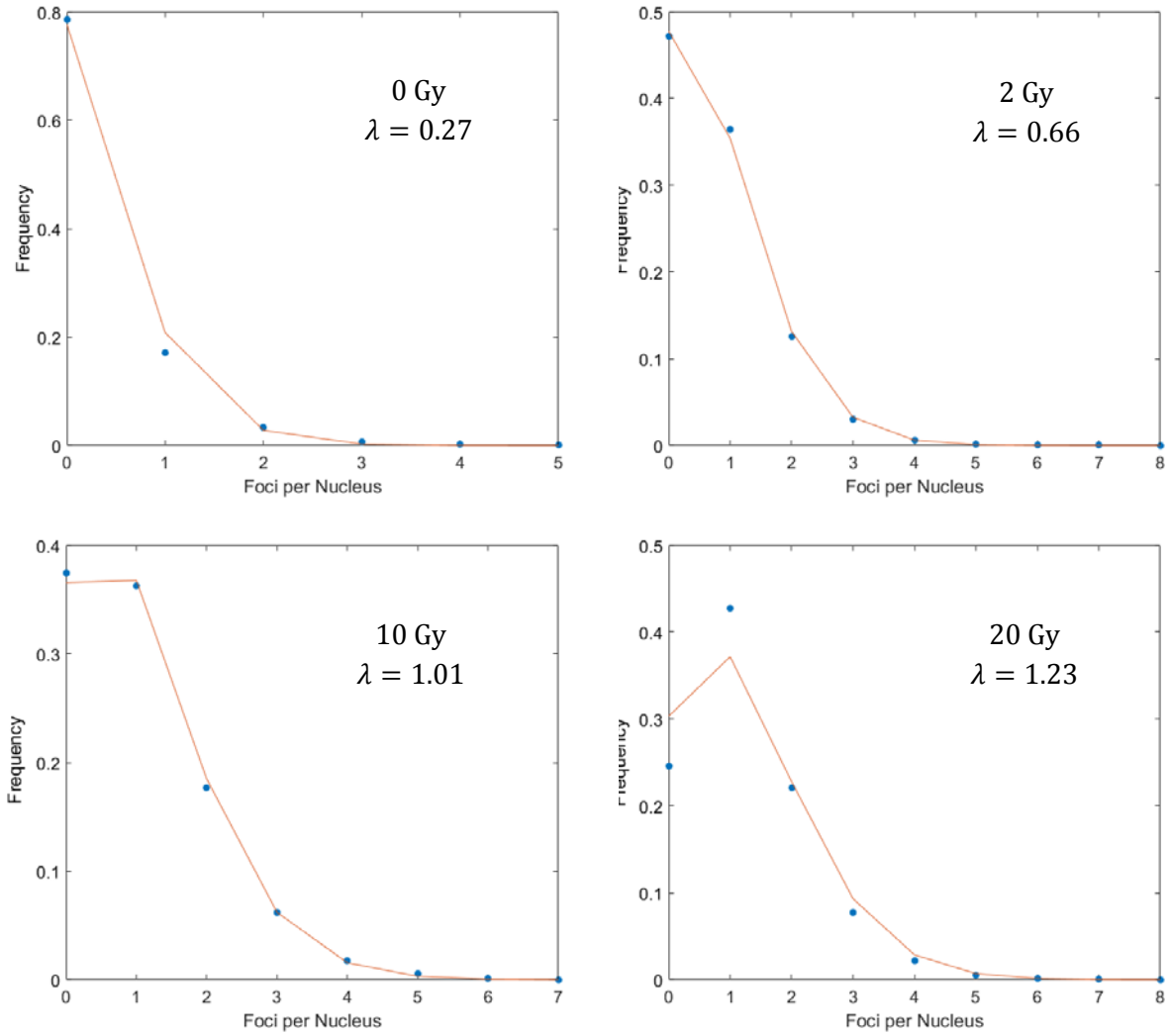

Figure 1. Frequency distributions for the number of foci per nucleus, for four dosage levels (blue). Theoretical Poisson distributions corresponding to sample means of count data (orange).

By inspection, the data are clearly Poissonian—equivalently, the quantile-quantile plots are highly linear (not pictured)—though the very large sample sizes preclude (and obviate) the use of a chi-squared test to corroborate this conclusion. However, an average of $\lambda = 0.27$ foci per nucleus in healthy, unirradiated neurons is certainly doubtful.[14] This may reflect any of several possible sources of error: 1) fluorescence background resulting from nonspecific binding of antibody; 2) processing artifacts leading to misidentification of foci; 3) processing artifacts leading to misidentification of nuclei. A combination of all three of these factors is likely.

Plotting the means by themselves reveals a nonlinearity in the low dose response, which is likely also an artifact of nonspecific puncta interpreted as γ-H2A.V foci. We may partially ameliorate this effect by choosing a different measure of γ-H2A.V: instead of the number of foci, we may choose instead to consider the size and fluorescence intensity (i.e., brightness). A simple way of doing this would be to integrate the intensity over the area of all identified γ-H2A.V foci in all identified nuclei. This approach yields a more linear dose curve with a lower basal signal, as can be seen by performing a linear fit to the data by least squares regression.

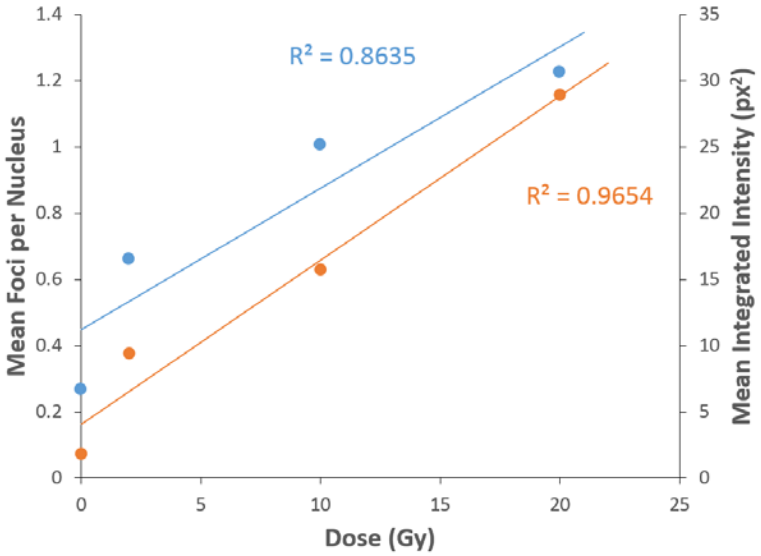

Figure 2. Two measures of γ-H2A.V abundance. Counts (blue) and integrated intensity (orange) at four dose levels, with trend lines and coefficients of determination.

A natural question that arises from the use of this integrated intensity metric is whether the two quantities that contribute to it—the size and intensity of the γ-H2A.V foci in each nucleus—are correlated. To test this hypothesis, we plotted focal area against mean focal intensity for each dose level and computed the Pearson correlation coefficient between the two parameters. Then, a linear regression analysis was performed in order to allow the degree of correlation to be visualized as a fit line.

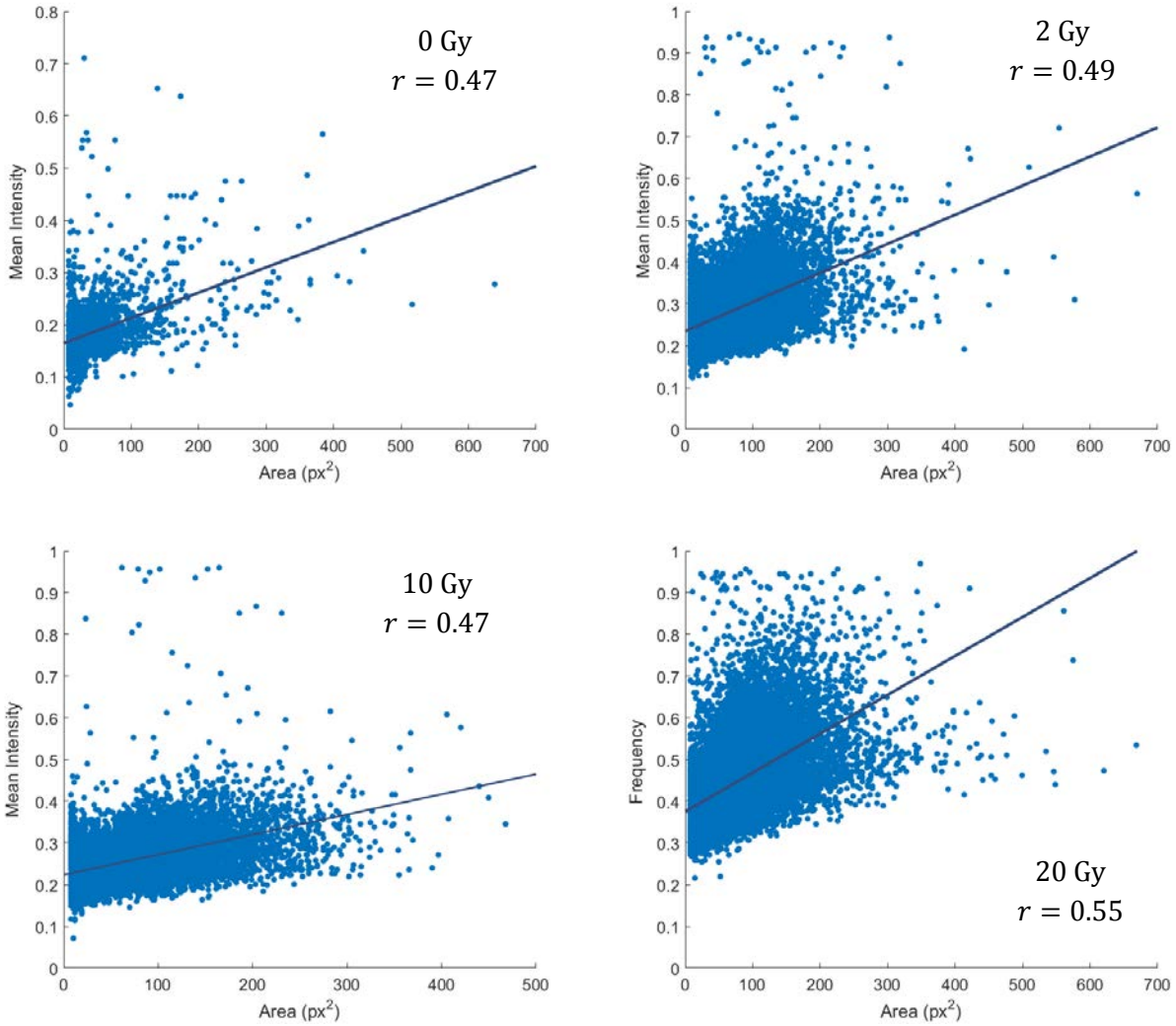

Figure 3. Scatter plots and value's of Pearson's *r* describing the correlation between the area and average intensity of γ-H2A.V foci, measured at four dose levels.

Evidently, the area of a γ-H2A.V focus is positively correlated with the mean intensity. This result captures an interesting feature of the distribution of γ-H2A.V molecules in the vicinity of a DSB. One possible interpretation is that repair foci increase in both size and histone concentration during the epoch immediately following upon DSB formation. This view is consistent with the positive-feedback model of γ-H2A.V-recruitment.[16]

On the whole, this case study illustrates the utility of quantitative image analysis as a technique for gaining insight into the physical processes that underlie biological phenomena. The

principal advantages of CellProfiler as a vehicle for image processing are: 1) modular design of processing pipelines allows for highly customizable workflows; 2) consolidated implementation of sophisticated segmentation and measurement algorithms that allow for extensive refinement of parameters; 3) substantially greater ease of creating robustly repeatable and reliably efficient workflows than with less-than-systematic application of individual tools, as in ImageJ. The second of these advantages is particularly remarkable, as I have encountered no other software packages that give such excellent results in declumping densely packed biological structures. To improve on CellProfiler's performance in this specific application, I suspect that it would be necessary to implement and modify many of the actual segmentation analysis steps myself.

References

1. Freitas AA, de Magalhães JP. A review and appraisal of the DNA damage theory of ageing. Mutat Res Rev Mutat Res. 2011;728(1-2):12–22.
2. Mehta A, Haber JE. Sources of DNA double-strand breaks and models of recombinational repair. Cold Spring Harb Perspect Biol. 2014;6(9):a016428.
3. Jackson SP. Sensing and repairing DNA double-strand breaks. Carcinogenesis. 2002;23(5):687–96.
4. Bassing CH, Alt FW. The cellular response to general and programmed DNA double strand breaks. DNA Repair. 2004;3(8-9):781–96.
5. Madigan JP, Chotkowski HL, Glaser RL. DNA double strand breaks-induced phosphorylation of *Drosophila* histone variant H2Av helps prevent radiation-induced apoptosis. Nucl Acids Res. 30(17)3698–705.
6. Aparicio T, Baer R, Gautier J. DNA double-strand break repair pathway choice and cancer. DNA Repair. 2014;19:169–75.
7. Khanna KK, Jackson SP. DNA double-strand breaks: signaling, repair and the cancer connection. Nat Genet. 2001;27(3):247–54.
8. Gorbunova V, Seluanov A. Making ends meet in old age: DSB repair and aging. Mech Ageing Dev. 20015;126(6-7):621–8.
9. Rass U, Ahel I, West SC. Defective DNA repair and neurodegenerative disease. Cell. 2007;130(6):991–1004.
10. Madabhusi R, Pan L, Tsai LH. DNA damage and its links to neurodegeneration. Neuron. 2014;83(2):266–82.

11. Jackson SP, Jeggo PA. DNA double-strand break repair and V(D)J recombination: involvement of DNA-PK. Trends Biochem Sci. 1995;20(10):412–5.
12. Heisig P. Type II topoisomerases—inhibitors, repair mechanisms, and mutations. Mutagenesis. 2009;24(6):465–9.
13. Sedelnikova OA, Rogakou EP, Panyutin IG, Bonner WM. Quantitative detection of ^{125}IdU-induced DNA double-strand breaks with γ -H2AX antibody. Radiat Res. 2002;158(4):486–92.
14. Rothkamm K, Löbrich M. Evidence for a lack of DNA double-strand break repair in human cells exposed to very low x-ray doses. Proc Natl Acad Sci U S A. 2003;100(9):5057–62.
15. Rogakou EP, Boon C, Redon C, Bonner WM. Megabase chromatin domains involved in DNA double-strand breaks *in vivo*. J Cell Biol. 1999;146(5):905–16.
16. Kinner A, Wu W, Staudt C, Iliakis G. γ-H2AX in recognition and signaling of DNA double-strand breaks in the context of chromatin. Nucl Acids Res. 2008;36(17):5678–94.
17. Hubbell JH. Photon mass attenuation and energy-absorption coefficients. Int J App Rad Isotop. 1982;33(11):1269–90.
18. Carpenter AE, Jones TR, Lamprecht MR, Clarke C, Kang IH, et al. CellProfiler: image analysis software for identifying and quantifying cell phenotypes. Genome Biol. 2006;7(10):R100.
19. Saisho Y, Ito A. Mathematical models of the generation of radiation-induced DNA double-strand breaks. J Math Biol. 2013;67(3):717–36.